http://journal.uir.ac.id/index.php/JGEET

E-ISSN : 2541-5794
P-ISSN : 2503-216X

Journal of Geoscience,
Engineering, Environment, and Technology
Vol 11 No 1 2026

RESEARCH ARTICLE

Unravelling the Sequence Stratigraphy Impact on Coal Geometry of M2 Member, Muara Enim Formation

Kevin Nabil Hibatullah [1], Budhi Setiawan[1], Yogie Zulkurnia Rochmana [1]*, M. Dwiki Satrio Wicaksono[2]

[1] *Geological Engineering Study Program, Engineering Faculty, Sriwijaya University, Indralaya, Ogan Ilir, South Sumatra 30862, Indonesia.*
[2] *PT. Bukit Asam Tbk., Jl. Parigi No.1., Tajung Enim, Muara Enim, South Sumatra 31716, Indonesia.*

* Corresponding author: yogie.zrochmana@ft.unsri.ac.id
Tel.:+6281234608055
Received: Jan 29, 2024; Accepted: Mar 13, 2026.
DOI: 10.25299/jgeet.2026.11.1.16191

Abstract

Sequence stratigraphy involves studying a series of rock layers deposited during a full change cycle in accommodation or sediment supply, bounded by subaerial unconformities and marine correlative conformities. This study aims to identify the stratigraphic sequence that controls the coal accumulation models and their influence on the coal geometry. The research methodology includes geological mapping, analysis of geophysical logs (gamma-ray and short density), and core log analysis. The data were analyzed, combined, interpreted, and simulated to create a model of coal accumulation and geometry. The M2 Member of the Muara Enim Formation comprises six lithofacies, as determined by analyzing four drill holes. The M2 Member of the Muara Enim Formation exhibits four depositional environments (crevasse splay, mire/swamp, mudflat, lagoon, and tidal/mouth/distal bar) and three facies associated with the fluvial delta–tidal plain facies (fluvial dominated upper delta plain, tide-dominated lower delta plain, and marginal tidal plain and lagoon). This research identified four system tracts, namely TST-1, HST-1, TST-2, and HST-2. TST-1 and TST-2 show continuous coal deposition, inclined to steeply inclined, interspersed, and characterized by the presence of three layers of clay bands. Similarly, HST-1 and HST-2 exhibit continuous coal deposition with gentle to steep inclined and interspersed, ranging from moderately thick to very thick, and containing one to five layers of clay bands. The tectonic activity after deposition caused the deposited coal to deform. The findings of this study contributed to guiding the exploration of coal seams in the South Sumatra Basin and Muara Enim Formation, in particular.

Keywords: Accumulation Model**,** Coal Geometry, Facies, Muara Enim Formation, Sequence Stratigraphy

1. Introduction

Sequence stratigraphy is defined as a succession of strata deposited during a complete cycle of change in accommodation or sediment supply, bounded by subaerial unconformities and their marine correlative conformities (Catuneanu et al., 2011; Ren et al., 2014) and can be divided into three discrete system tracts such as lowstand, transgressive, and highstand system tracts (Ren et al., 2014; Wagoner et al., 1990a). Coal seam geometry is an aspect of the dimensions or size of a coal seam that includes thickness, dip, and continuity (Marcelino, 2016; M.L. Jeremic, 1985). The coal accumulation model is proposed by analyzing the stratigraphic framework and lithofacies characteristics of the sequence (Duan et al., 2021).

The research area is located geographically in Tanjung Enim, Muara Enim Regency, South Sumatra, within the Muara Enim Formation (**Fig. 1**). This coal-bearing formation was deposited during the Late Miocene to Early Pliocene and consists of claystones, siltstones, sandstone, and coal (Amijaya and Littke, 2005) The formation is divided into two members: Lower MPa (Middle Palembang 'a') and Upper MPb (Middle Palembang 'b'). Both members have been subdivided into M1-M4 (Amijaya and Littke, 2005; Shell Mijnbouw, 1976).

However, most studies have focused on facies, depositional environments, and geometry. Previous research subdivided the depositional environment into ombrotrophic and mesotrophic in telmatic and limno-telmatic conditions based on maceral assemblages using tissue preservation and gelification index, as well as vegetation and groundwater index (Amijaya and Littke, 2005). In a separate study, the Muara Enim Formation was deposited in various environments, including the lower delta plain, transitional lower delta plain, and upper delta plain. The Upper Muara Enim Formation comprises six sediment facies: peat swamp, distributary channel, floodplain, mudflat, mixed flat, and mouth bar (Elcofa et al., 2023). The thickness of coal seams from A1 to D in the Muara Enim Formation ranges from 1.65 to 12 meters (Algadri Nafian and Rizal, 2021). Coal seams are generally continuous, controlled by fluvial and structural processes, such as folding (horseback), and faulting (Kurniawan, 2021).

Few prior studies have comprehensively examined the correlation between sequence analysis and coal geometry in this area. Therefore, research that focuses on the M2 Member of the Muara Enim formation will significantly contribute to understanding how the stratigraphic sequence influences the distribution and geometry of coal accumulation.

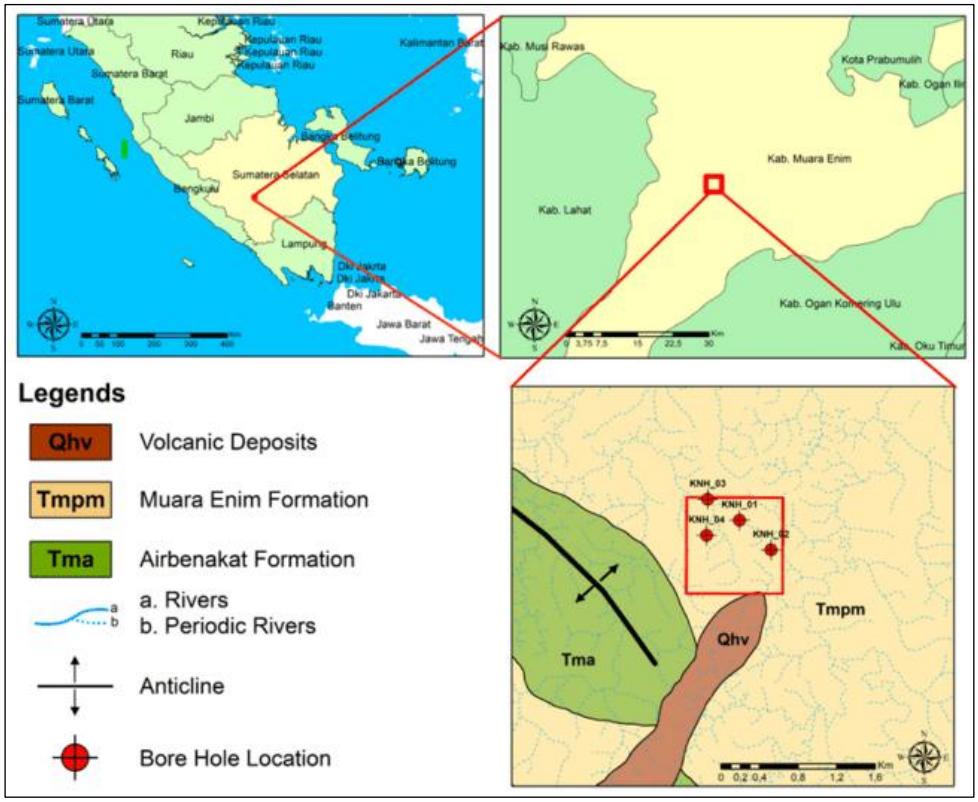

Fig 1. Maps of the research area.

2. Materials and Method

The research methodology employed in this study encompasses geological mapping, geophysical logging, and core log analysis (**Fig. 2**). Geological mapping involves describing rock outcrops and collecting rock samples to provide a detailed depiction of the geological conditions found in the outcrops (Adam and Rochmana, 2022). The collection of geological structure data helps to understand the tectonic influence on the stratigraphic order at the research location. This methodology is crucial for gaining insight into the study area's tectonic history and geological characteristics. It establishes the basis for the subsequent analysis and interpretation of the data collected.

The analysis of lithofacies and sedimentary facies, parasequence and parasequence sets, system tracts, and stratigraphic sequences was conducted based on geophysical log and core log datasets from four drill holes (**Fig. 2**). Facies types were identified using core log data, while the lithofacies table from Wang et al., (2011) was used to determine lithofacies and sedimentary facies.

Certain patterns in geophysical logs reflect different sedimentation processes. When interpreting geophysical log curves, the geophysical curve pattern is classified by (Walker and James, 1992) is used. Parasequence and parasequence set boundaries in each drill hole are identified based on the presence of a flooding surface that separates marine and terrestrial sediments (Wagoner et al., 1990b). These boundaries are shown by significant changes in the log pattern (Bai et al., 2020). The system tracts comprising the stratigraphic sequence in each drill hole are identified based on the explanation provided by Catuneanu, (2020), Catuneanu (2017), and Catuneanu et al., (2011).

The geological cross-section model depicting the coal geometry and accumulation model in the research area was created by integrating four geophysical logs and core logs datasets. Isopach maps of coal distribution and 3D modeling were interpolated using the Inverse Distance Weighting (IDW) interpolation method. The Inverse Distance Weighting (IDW) interpolation is a commonly used technique for estimating values in unsampled areas by calculating a weighted average of the known values within the neighborhood. (Herrero-Hernández et al., 2017).

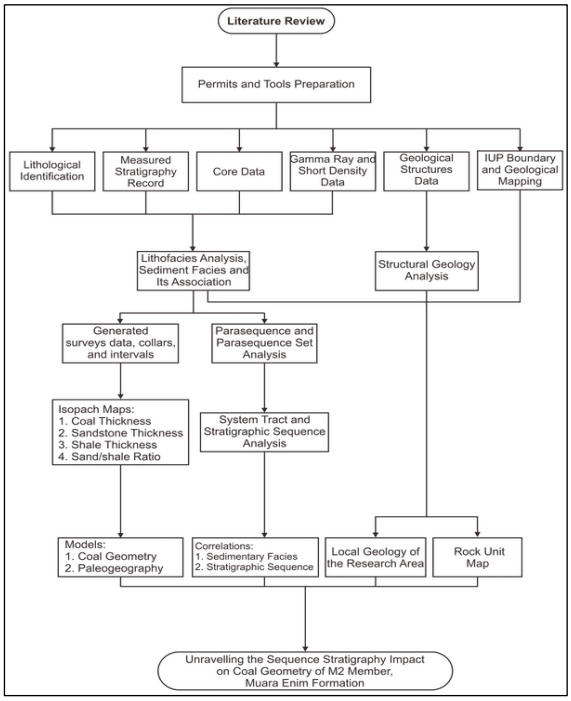

Fig. 2 . Flowchart of research methodology illustrating data acquisition, data analysis, and results

3. Results

3. 1 Lithofacies Analysis

Based on the four drill holes data that have been analyzed, six lithofacies of the M2 Member of the Muara Enim Formation found in the research area are shown in **Fig. 3** and summarized in **Table 1**.

Table 1. Lithofacies that identified in the research area.

Lithofacies	Descriptions	Sedimentary Structures	Sub Facies/ Depositional Environment	Genesis
Tuffaceous sandstone and tuffaceous clay-stone interspersed	Tuffaceous sandstone and tuffaceous claystone interspersed on top	Bedding, lamination	Crevasse splay	Interbedding happened when volcanic material in floodplain areas of rivers or deltas is carried away by river currents that are full of clay material during overflow (Lepre, 2017).
Glauconitic sandstone	Fine glauconitic sandstone	Lamination, wavy bedding, flaser bedding	Tidal/mouth/ distal bars	Formed by strong tidal currents, either in one or two directions with thin claystone inserts carried by the same currents (Olariu et al., 2012).
Shale with lenses and siderite bands or nodules	Dark grey shale interspersed with sand-stone	Lenticular bedding	Tidal flats	Formed in shallow environments such as poorly sorted mixed systems, and was influenced by transgression-regression cycles, exhibiting a strong marine influence (Tang et al., 2023).
Dark grey claystone	Brownish-dark grey claystone consists of siderite bands	Lamination, massive	Lagoon	Siderite lamination characterizes the cyclic direct deposition of iron-rich seawater under reducing conditions in an organic-rich and acidic environment (Lukoczki et al., 2015).
Carbonaceous claystone/ mudstone	Black claystone, rich of carbon contents	Massive	Mire	The deposit comprises organic material and is formed by processes involving both reversing and unidirectional tidal currents. (Shao et al., 2015).
Coal	Black, bright-dull, consist of 3-5 layers of clay bands	Banded	Mire	Vegetable debris accumulates in a specialized deposition environment (Thomas, 2020). Deposition stops when the debris is buried under sediments. Over time, with exposure to heat and pressure, the debris transforms into coal. (Arnold, 2013; ISO, 2005).

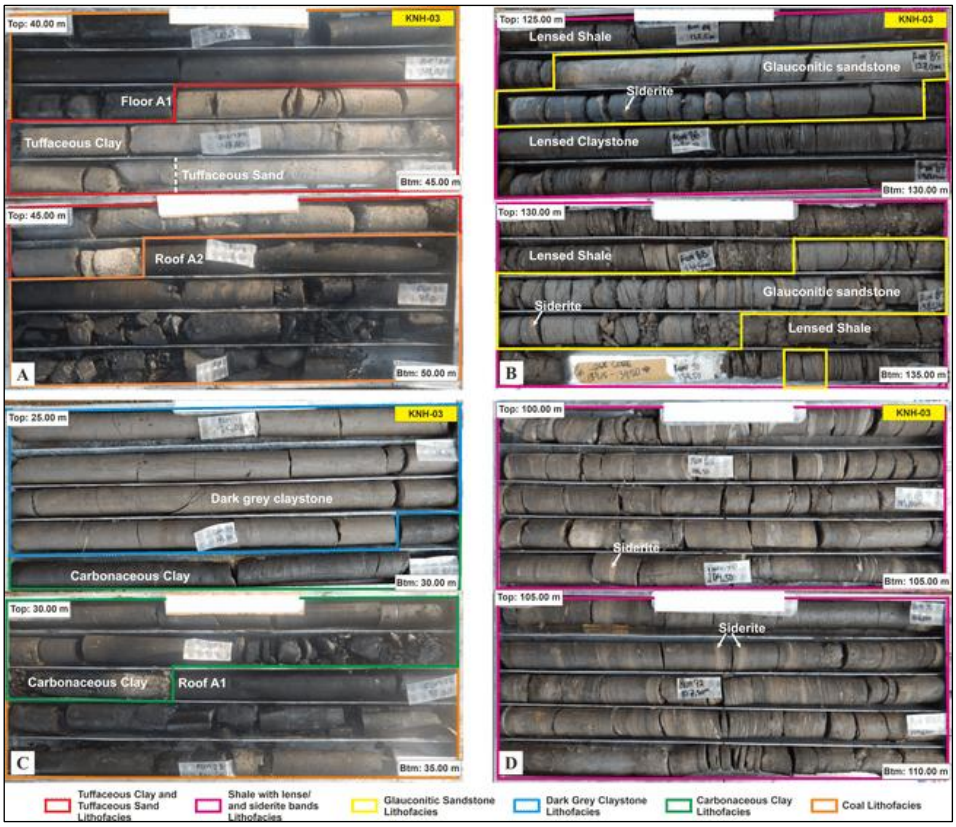

Fig. 3 Core pictures from KNH-03 of six lithofacies found in the research area: A) Tuffaceous clay and tuffaceous sandstone interspersed facies and coal facies (seam A1 & A2); B) Glauconitic sandstone facies and shale facies with lenses and siderite bands/nodules; C) Dark grey claystone facies, carbonaceous claystone facies, and coal facies; D) Shale facies consist of siderite bands.

3. 2 Identification of System Tracts and Stratigraphic Sequence Boundaries

The stratigraphic sequence comprises of Lowstand System Tract (LST), Transgressive System Tract (TST), and Highstand System Tract (HST). Determining the Maximum Flooding Surface (MFS) as the system tract boundary and sequence boundary (SB) is the main key, which can be demonstrated by significant changes in the geophysical log (gamma-ray) curve pattern and lithology (Ren et al., 2014). The interpretation of stratigraphic sequence boundaries in the study area is based on facies associations and marine deposits as boundary markers (Wang et al., 2011). In this study, sandstone, which is a characteristic of shallower area sedimentary material, is overlain by dark claystone or shale, which characterizes deeper marine sediment, identified as the marine flooding surface (Wagoner et al., 1990b, 1990a). The Maximum Flooding Surface (MFS) can be interpreted as a significant change from TST to HST.

3. 2. 1 Sequence 1

Sequence 1 in the research area comprises two system tracts, namely the transgressive system tract (TST-1) and the highstand system tract (HST-1), which is bounded by Maximum Flooding Surface 1 (MFS-1) (Fig. 4 and **Fig. 6**). The boundary between these two system tracts was identified based on the dominant pattern in the parasequence set and the marine flooding surface, which indicates clear lithological changes between terrestrial deposits and shallow marine deposits. At the research location, the transgressive system tract (TST-1) exhibits a low sand/shale ratio. This system tract is characterized by interspersed lagoon deposits consisting of dark gray shale (Lukoczki et al., 2015). and carbonaceous claystone facies (Dill et al., 1997), as well as coal facies (seam C), as mire deposits that were deposited in the marginal tidal plain and lagoon facies.

TST-1 is characterized by the accumulation of thick, dark, shallow marine and swamp sedimentary materials, such as dark gray shale and carbonaceous claystone. The system tract is marked by the presence of sets with a bell curve pattern, indicating a succession of fining upward lagoonal shale, and sets with a cylindrical pattern, providing evidence of aggradation parasequence sets that accumulate seam C.

Late TST-1 and the initial HST-1 are bounded by MFS-1, which had the highest water level at the research location during that time (**Fig. 4** and **Fig. 6**). MFS-1 exhibits changes in the coastline from transgression towards normal highstand regression (Zhang et al., 2020). In the gamma-ray log, MFS-1 was identified by a change in the dominant retrogradation-aggradation stacking pattern towards a progradation stacking pattern. Based on the core analysis, MFS-1 is characterized by a clear lithological shift that bounds the lagoon deposits, forming a dark gray shale overlain by tidal flat deposits above, which consist of lensed glauconitic sandstone facies.

The Highstand System Tract of sequence 1 (HST-1) was deposited above MFS-1. MFS-1 is characterized by an increase in the sand/shale ratio compared to TST-1. Deposition of glauconitic sandstone began on HST-1. Glauconite indicates shallow marine deposits (Torrado et al., 2020).

HST-1 is characterized by the intercalated deposition of marine material in the form of shale and glauconite sandstone with a tidal bedding structure. The shale is dark gray, lensed, and very thick with siderite bands and nodules. The glauconitic sandstone is bright greenish-gray and has very fine sand grains with a tidal bedding structure (flaser bedding and wavy bedding). These lithofacies were deposited in a marginal tidal plain and lagoon–tide dominated lower delta plain facies with tidal/mouth/distal bar–tidal flat sub-facies.

The gamma-ray log analysis on HST-1 shows the recurrence of coarsening upward parasequences, which then form a set of progradation parasequences because the rate of sediment supply is greater than the rate of increase in accommodation space.

The occurrence of repeated coarsening-upward parasequences, as shown by the funnel-shaped gamma-ray curve, and followed by the presence of a cylindrical pattern that accumulates seam B2, formed the aggradation parasequence set. Sequence Boundary 1 (SB-1), as shown in **Fig. 4** & **Fig. 6**, marks the end of HST-1. SB-1 was formed due to a relatively rapid decrease in sea level with a small sediment supply (Wagoner et al., 1990b). SB-1 represents an unconformity plane caused by an erosional period that bounds sequences 1 and 2. The paleography map of Sequence 2 is shown in **Fig. 5a**.

3. 2. 2 Sequence 2

Sequence 2 is formed through a mechanism similar to sequence 1. It consists of two system tracts, which start with TST-2 and HST-2 and are bounded by SB-1 at the bottom and SB-2 at the top (**Fig. 4**).

Transgressive system tract sequence 2 (TST-2) is bounded by SB-1 at the bottom and MFS-2 at the top. TST-2 is characterized by a decrease in the sand/shale ratio and the dominance of interspersed lagoon deposits (claystone) with mire deposits (coal). In contrast to TST-1, carbonaceous claystone facies were not deposited in TST-2. The dominant lithofacies deposited in TST-2 are laminated claystone with bands of siderite and coal, characteristic of the marginal tidal plain and lagoon facies.

The gamma-ray log displays TST-2 through the accumulation of fining-upward parasequences, which are composed of laminated claystone and exhibit a bell curve pattern. Aggradational parasequences are also present, showing the accumulation of seam B1, Suban Marker, and A2. TST-2 is characterized by a retrogradation parasequence set, resulting from an increase in water level, which creates a larger accommodation space compared to the sediment supply.

From the end of TST-2 to the beginning of HST-2, there was a significant rise in sea level. The accommodation space formed at the end of TST-2 was large, but the rate of accommodation space formation was balanced by the rate of peat accumulation; many coal-forming plants thrived, and peat accumulation occurred (Xu et al., 2020). MFS-2 shows a transition in the coastline from transgression towards normal highstand regression (Zhang et al., 2020). MFS-2 was identified by a change in the dominant

retrogradation-aggradation stacking pattern to a progradation stacking pattern (**Fig. 6**).

Highstand system tract sequence 2 (HST-2) is bounded by MFS-2 at the bottom and SB-2 at the top. HST-2 began with the deposition of the crevasse splay facies, consisting of tuffaceous sandstone overlain by tuffaceous claystone, due to river currents overflowing with clay materials. This system tract experienced a subsequent rise in the sand/shale ratio and an increase in marine sediment thickness, particularly after MFS-2.

HST-2 is characterized by lagoon deposits composed of massive dark gray claystone and mire deposits consisting of massive carbonaceous claystone and coal with clay band impurities, which were formed in the mire environment of the marginal tidal plain and lagoon–fluvial dominated upper delta plain facies. Gamma-ray log analysis of HST-2 reveals retrogradation and aggradation parasequences, forming a set of aggradation parasequences characteristic of HST-2.

HST-2 is characterized by a coarsening-upward pattern, as indicated by sets of bell-shaped gamma ray curves and a cylindrical curve pattern, which shows an aggradational parasequence that accumulated seam A1. The end of HST-2 is designated as Sequence Boundary 2 (SB-2) and is marked by the contact between the claystone and the overlying soil. SB-2 is an erosional unconformity that formed in response to a relatively rapid sea level fall with a limited sediment supply (Wagoner et al., 1990b). The Paleography map of Sequence 2 is shown in **Fig. 5b**.

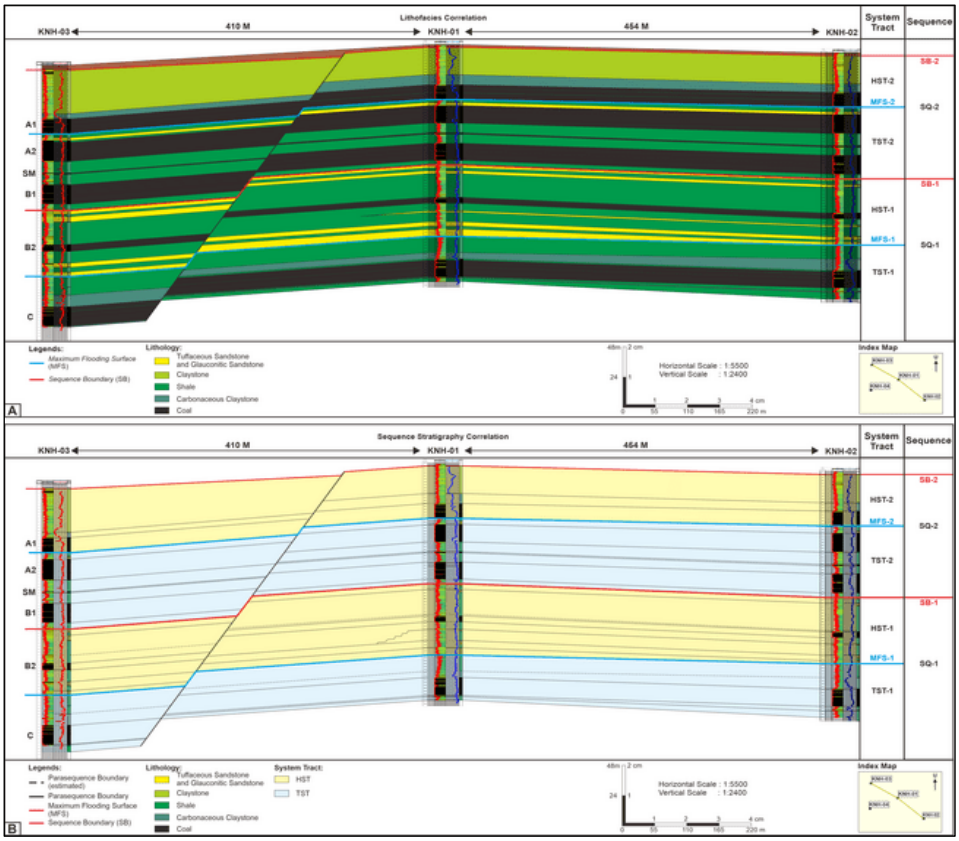

Fig. 4. A) Lithofacies correlation in the research area, which is correlated from three drill holes data parallel to strike direction, with structure influence; B) Stratigraphic sequence and system tract in the research area, which is correlated from drill holes data parallel to strike direction with structure influence.

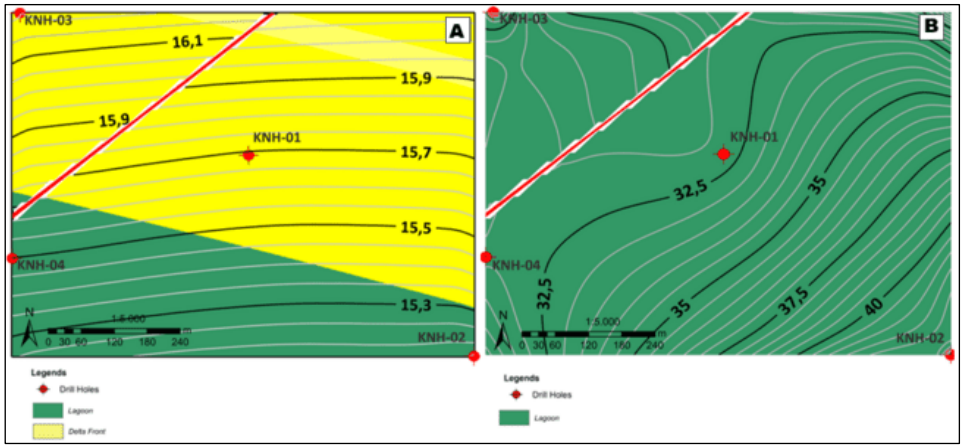

Fig. 5. A) Paleogeography map of Sequence 1; B) Paleogeography map of Sequence 2

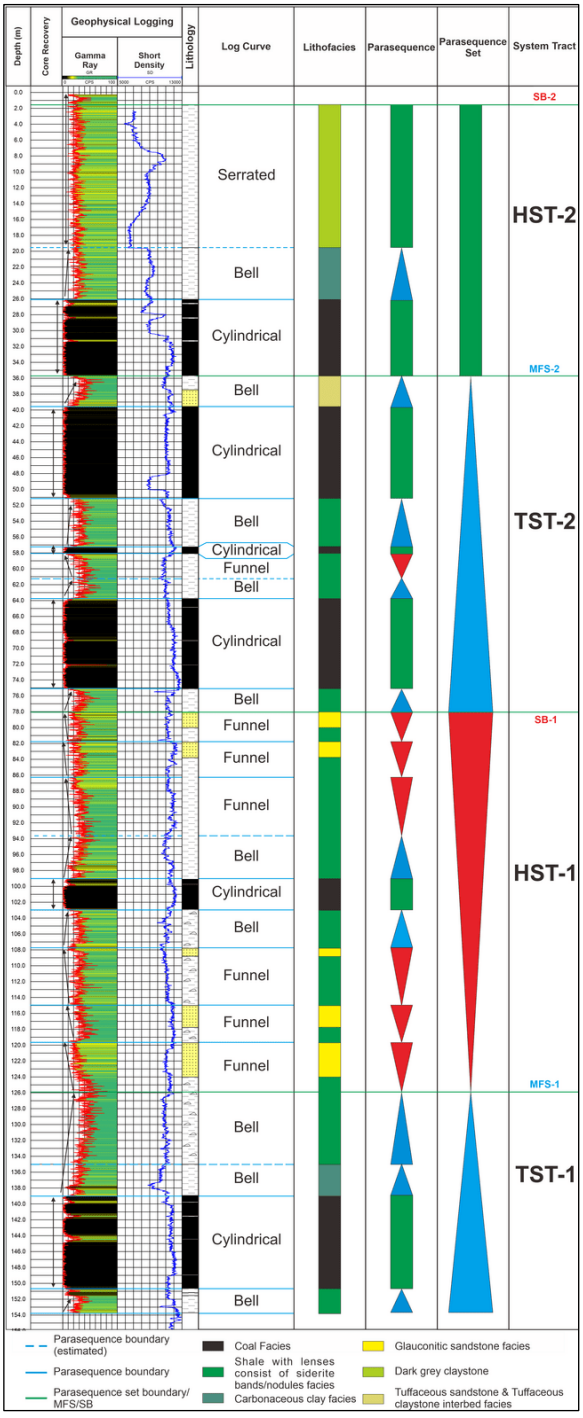

Fig. 6. Analysis of parasequence and parasequence sets and system tracts identification of TST-1, HST-1, TST-2, and HST-2 of KNH-01 drill hole.

3.3 Distribution and Coal Geometry of the Muara Enim Formation

3. 3. 1 Sequence 1

TST-1 is the first depositional mechanism in the research area that deposited the coal seam C. The coal deposited in this system tract has continuous geometric features (>1 km) as observed in **Fig. 3B**, very thick (11.35-12.00 m), tilted (20◦), and interspersed by the presence of four layers of clay bands (**Fig. 6**). The interspersed clay bands in the coal body are interpreted as evidence of paleoclimatic changes during coal deposition (Hou et al., 2023) and influenced by sea-level fluctuations during the transgression.

The isopach map of Seam C in TST-1 (**Fig. 7A**) was created to show the distribution of coal and the areas that were centers of coal accumulation during this period, as well as to reflect the distribution of swamp/mire areas. From the isopach map, it can be concluded that the center of thick coal accumulation is located at KNH-03 (northwest) with a coal thickness of over 11 m, and becomes thinner at KNH-02 (southeast). It can also be interpreted that the northwest is terrestrial and the southeast is marine.

Seam B2 was deposited during the HST-1 period. The coal seam B2 has continuous geometric characteristics, is moderately thick (3.72-4.30 m), gently inclined (18◦), and is interspersed with 1 layer of clay band. Clayband is an indicator that sea level rise brought clay material from the marine environment to the mire/swamp, which temporarily halted coal accumulation during HST-1.

The isopach map of seam B2 (**Fig. 7B**) shows the distribution pattern of seam B2. It can be observed that the coal distribution pattern has narrowed compared to the distribution of seam C, which was previously formed in TST-1. This is due to the increase in seawater, which results in more accommodation space compared to the supply of coal-forming sediment. The coal accumulation process is interrupted by the predominant accumulation of sands and clays, so that the coal formed is not too thick compared to the C seam coal formed during TST-1.

Based on the isopach map, it can be seen that the depositional environment during this period was dominated by the tidal flat–tidal/mouth/distal bar, which is represented by the gray–white area on the map. The center of coal accumulation is represented by a dark gray-black area located in the northwest direction (KNH-03) of the study area with a coal thickness of over 4m.

3. 3. 2 Sequence 2

Sequence 2, consisting of TST-2 and HST-2, is the most important depositional system that accumulates coal seams at the research location. TST-2 is a system tract that deposited two main seams, seam B1 and seam A2, and one thin, Suban Marker. Meanwhile, HST-2 is a system tract that deposits seam A1.

Seam B1 is the first seam formed as a result of the TST-2 mechanism, which is deposited continuously (>1 km), very thick (11.10-12.46 m), gently inclined (18◦), and contains clay band impurities. A total of 5 clayband layers formed show the intensity/frequency of seawater fluctuations (repeated transgression-regression mechanism), which interrupted the B1 coal accumulation process at the research site during the TST-2 period. Very thick coal is formed because the sediment supply forming the coal is greater than the accommodation space formed. Based on the B1 isopach map (**Fig. 7C**), it can be inferred that the distribution of thick coal thickness occurs in a northeast–southwest direction, with coal accumulation centers located at KNH-01, KNH-02, and KNH-03.

Suban Marker is a thin coal with a thickness ranging from 0.60-0.84 m, continuous (>1Km), steeply inclined 16˚), without any interruption. Based on these geometric characteristics, it is inferred that this coal was formed when the supply of coal-forming sediment exceeded the

accommodation space for a short period. The Suban Marker isopach map (**Fig. 7D**) shows how the distribution of the Suban Marker is formed, where the center of accumulation is in the middle of the map, precisely at KNH-01 and KNH-02 with northwest-southeast orientation.

Seam A2 was formed during the early TST-2 period. This coal has the geometric characteristics of being very thick (11.48-13.38 m), deposited continuously (>1 km), steeply inclined (14˚), with three layers of clay band impurities, which indicates the intensity of seawater fluctuations disturbance during the accumulation of Seam A2. Based on the A2 isopach map (**Fig. 7E**), the thick coal distribution pattern is shown in a northwest-southeast direction, with the center of coal accumulation at the KNH-01, KNH-02, and KNH-03 drill holes. Towards the southwest, the coal thickness decreases.

Seam A1 is a coal body deposited at the end of TST-2 and the beginning of HST-2. Seam A1 has a thickness variation of 9.40-9.60 m, is continuous (>1km), gently inclined (14˚), and contains three layers of clay band contamination. Clay bands indicate that rising sea levels brought clay material from the sea to the marsh, which covered the underlying coal during HST-2.

In the isopach map of Seam A1 (**Fig. 7F**), it was observed that the coal distribution pattern expanded after TST-2. The center of the coal accumulation is located at KNH-01, KNH-02, and KNH-03, which is wider than the accumulation during HST-1. During a period of high water table in the swamps, followed by a stable water table, a large amount of peat accumulated (Abidin et al., 2022).

After coal accumulation ceased in the Late Miocene-Pliocene, post-depositional tectonic activity led to the deformation of the deposited coal. **Figure 8** shows the brittle and ductile deformation indicated by the fault structure and monocline folds affecting the coal geometry.

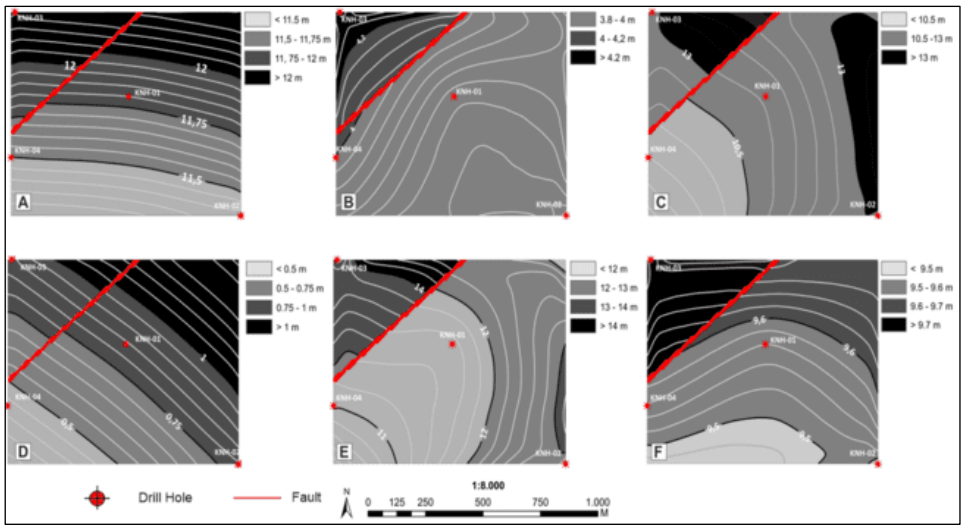

Fig 7. Isopach maps of coal thickness: a) Seam C of TST-1; b) Seam B2 of HST-1; c) Seam B1 of TST-2; d) Suban Marker of TST-2; e) Seam A2 of TST-2; f) Seam A1 of HST-2.

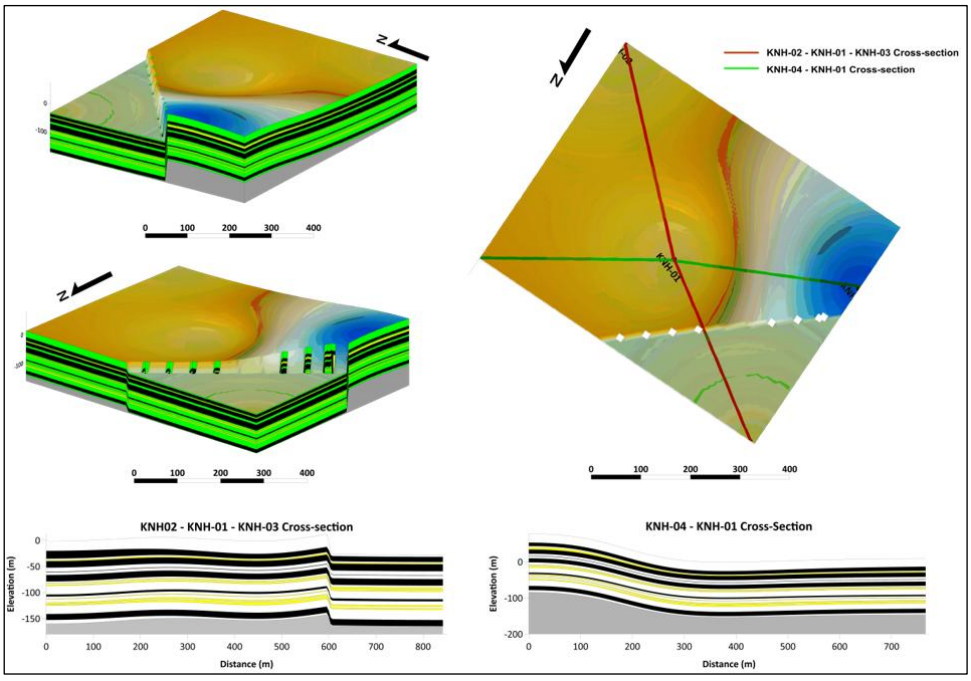

Fig 8. 3D model of coal geometry and distribution, and cross-section.

Table 2. Summary of the stratigraphic sequence and geometry of each seam in the study area.

Seam	Coal Thickness		Coal Thickness		Continuity	Dip
	TST-1	HST-1	TST-2	HST-2		
C	11.35-12.00	-	-	-	Continuous	20°
B2	-	3.00-4.10	-	-	Continuous	18°
B1	-	-	11.1-12.46	-	Continuous	18°
Suban Marker	-	-	0.60-0.84	-	Continuous	14 °
A2	-	-	11.48-13.38	-	Continuous	14°
A1	-	-	-	9.40-9.60	Continuous	14°

Based on the results of this study, the sedimentary facies of the M2 Member of the Muara Enim Formation are classified into four sedimentary facies consisting of fluvial-dominated upper delta plain, fluvial/tidal transitional delta plain, tidal-dominated lower delta plain, and marginal tidal plain and lagoon. This is different from the findings of previous researchers, such as Amijaya and Littke, (2005) who divided the depositional environments into ombrotrophic and mesotrophic into telmatic and limno-telmatic conditions, or Elcofa et al., (2023) who divided the sedimentary facies/environments into six categories, namely peat swamp, distributary channel, floodplain, mudflat, mixed flat, and mouth bar.

From this research result, the coal thickness ranges from 0.60-0.84 m (thinnest) to 13.38 m (thickest), which is slightly different from the coal thickness found by Algadri Nafian and Rizal (2021). The coal is deformed (faulted and folded) into a monocline fold (horseback) due to the impact of the geological structure, as modeled. This discovery is consistent with the findings of Kurniawan (2021).

4. Conclusion

The study area consists of four depositional environments (crevasse splay, mire/swamp, mudflat, lagoon, and tidal/mouth/distal bar) and three facies associated with the fluvial delta–tidal plain facies (fluvial dominated upper delta plain, tide-dominated lower delta plain, and marginal tidal plain and lagoon).

The depositional process in the study area consists of two stratigraphic sequences (Sequence 1 and Sequence 2), each consisting of a Highstand System Tract (HST) and a Transgressive System Tract (TST). The end of the TST and the beginning of the HST are bounded by the Maximum Flood Surface (MFS), while the end of the HST and the beginning of the TST are bounded by the Sequence Boundary (SB).

Overall, both Sequence 1 and Sequence 2 produce identical coal geometry in the study area, which is thick, continuous, and contains clay bands with an average dip of 16-17◦. The structure's influence results in the coal's folding and faulting.

Acknowledgements

The author would like to thank PT. Bukit Asam Tbk for the support in terms of facilities and legal permissions that contributed to this research.

References

Abidin, N.S.Z., Mustapha, K.A., Abdullah, W.H., Konjing, Z., 2022. Paleoenvironment Reconstruction and Peat-Forming Conditions of Neogene Paralic Coal Sequences from Mukah, Sarawak, Malaysia. Sci Rep 12, 1–26. https://doi.org/10.1038/s41598-022-12668-6

Adam, M.D.K., Rochmana, Y.Z., 2022. Analisis Stratigrafi dan Sejarah Pengendapan Daerah Cibenda, Kabupaten Ciamis, Jawa Barat Dan Sekitarnya. Jurnal Geologi Terapan Ophiolite 4, 69–83.

Algadri Nafian, M., Rizal, Y., 2021. Geologi Batubara Daerah Tanjung Enim, Kabupaten Muara Enim, Provinsi Sumatera Selatan. Bulletin of Geology 5, 589. https://doi.org/10.5614/bull.geol.2021.5.2.3

Amijaya, H., Littke, R., 2005. Microfacies and Depositional Environment of Tertiary Tanjung Enim Low Rank Coal, South Sumatra Basin, Indonesia. Int J Coal Geol 61, 197–221. https://doi.org/10.1016/j.coal.2004.07.004

Arnold, B.J., 2013. Coal Formation. The Coal Handbook: Towards Cleaner Production 1, 31–52. https://doi.org/10.1533/9780857097309.1.31

Bai, Y., Lü, Q., Liu, Z., Sun, P., Liu, R., Yao, S., 2020. Coal-Bearing Strata Sequence Stratigraphy of Paleogene Meihe Formation, Meihe Basin, NE China. Int J Coal Sci Technol 8, 547–561. https://doi.org/10.1007/s40789-020-00381-6

Catuneanu, O., 2020. Sequence Stratigraphy in The Context of the 'Modeling Revolution.' Mar Pet Geol 116. https://doi.org/10.1016/j.marpetgeo.2020.104309

Catuneanu, O., 2017. Sequence Stratigraphy: Guidelines for a Standard Methodology. pp. 1–57. https://doi.org/10.1016/bs.sats.2017.07.003

Catuneanu, O., Galloway, W.E., Kendall, C.G.S.C., Miall, A.D., Posamentier, H.W., Strasser, A., Tucker, M.E., 2011. Sequence Stratigraphy: Methodology and Nomenclature. Newsl Stratigr 44, 173–245. https://doi.org/10.1127/0078-0421/2011/0011

Dill, H. G., Scheel, M., Köthe, A., Botz, R., & Henjes-Kunst, F. (1997). An integrated environment analysis—lithofacies, chemofacies, biofacies—of the Oligocene calcareous-siliciclastic shelf deposits in northern Germany. *Palaeogeography, Palaeoclimatology, Palaeoecology*, *131*(1), 145–174.https://doi.org/https://doi.org/10.1016/S0031-0182(96)00141-1

Duan, H., Xie, W., Zhao, J., Jia, T., 2021. Sequence Stratigraphy and Coal Accumulation Model of The Taiyuan Formation in the Tashan Mine, Datong Basin, China. Open Geosciences 13, 1259–1272. https://doi.org/10.1515/geo-2020-0303

Elcofa, D.G., Rochmana, Y.Z., Hastuti, E.W.D., Gibran, M.A.K., 2023. Identifikasi Suksesi Delta Formasi Muaraenim Atas Daerah Tanjung Enim, Sumatera Selatan. Journal of Geology Sriwijaya 2, 1–5.

Herrero-Hernández, A., López-Moro, F.J., Valle-Feijóo, M.E., Gómez-Fernández, F., Rodríguez-Pérez, J.R., 2017. Mapping of Tecto-Lineaments and Their Influence on Sedimentological Processes in a GIS Environment: A Case Study of the Iberian Trough, Spain. Geologica Carpathica 68, 165–174. https://doi.org/10.1515/geoca-2017-0013

Hou, H., Shao, L., Tang, Y., Li, Y., Liang, G., Xin, Y., Zhang, J., 2023. Coal Seam Correlation in Terrestrial Basins by Sequence Stratigraphy and Its Implications for Paleoclimate and Paleoenvironment Evolution. Journal of Earth Science 34, 556–570. https://doi.org/10.1007/s12583-020-1069-4

International Standards Organization, 2005. Classification of Coals.

Kurniawan, P., 2021. Coal Geometry Modeling and Resources Estimation in Darmo and Surrounding Area, Muara Enim, South Sumatra. Indonesian Journal of Economic Geology 1, 85–91. https://doi.org/10.51835/ijeg.2021.1.1.344

Lepre, C.J., 2017. Crevasse-Splay and Associated Depositional Environments of the Hominin-Bearing Lower Okote Member, Koobi Fora Formation (Plio-Pleistocene), Kenya. The Depositional Record 3, 161–186. https://doi.org/10.1002/dep2.31

Lukoczki, G., Budai, T., Németh, T., 2015. Sideritic-Kaolinitic and Green Clay Layers in The Mecsek Mountains (SW Hungary): Indicators of Middle Triassic Volcanism-Myth or Reality? Central European Geology 58, 334–355. https://doi.org/10.1556/24.58.2015.4.4

Marcelino, N.Y., 2016. Geologi dan Potensi Batubara di Daerah Bonggo dan Sekitarnya Kabupaten Jayapura, Provinsi Papua. Promine Journal 4, 1–7.

M.L. Jeremic, 1985. Strata Mechanics in Coal Mining, 1st ed. A.A.Balkema Publishers, Rotterdam. https://doi.org/https://doi.org/10.1201/9781003079170

Olariu, M.I., Olariu, C., Steel, R.J., Dalrymple, R.W., Martinius, A.W., 2012. Anatomy of a laterally migrating tidal bar in front of a delta system: Esdolomada Member, Roda Formation, Tremp-Graus Basin, Spain. Sedimentology 59, 356–378. https://doi.org/10.1111/j.1365-3091.2011.01253.x

Ren, J., Wang, H., Sun, M., Gan, H., Song, G., Sun, Z., 2014. Sequence Stratigraphy and Sedimentary Facies of Lower Oligocene Yacheng Formation in Seepwater Area of Qiongdongnan Basin, Northern South China Sea: Implications for Coal-Bearing Source Rocks. Journal of Earth Science 25, 871–883. https://doi.org/10.1007/s12583-014-0479-6

Shao, L.Y., Yang, Z.Y., Shang, X.X., Xiao, Z.H., Wang, S., Zhang, W.L., Zheng, M.Q., Lu, J., 2015. Lithofacies palaeogeography of the Carboniferous and Permian in the Qinshui Basin, Shanxi Province, China. Journal of Palaeogeography 4, 384–412. https://doi.org/10.1016/j.jop.2015.06.001

Shell Mijnbouw, N.V., 1976. Geological Study of the Bukit Asam Coal Mines. Jakarta.

Tang, H., Zhao, Q., Liu, B., Tan, S., Shi, K., 2023. Types and Genesis of Siderite in the Coal-Bearing Beds of the Late Permian Xuanwei Formation in Eastern Yunnan, China. Minerals 13. https://doi.org/10.3390/min13091233

Thomas, L. (Larry P.), 2020. Origin of Coal, in: Coal Geology. John Wiley & Sons, Abergavenny, pp. 5–55.

Torrado, L., Arenas, L.C.C., Mann, P., Bhattacharya, J., 2020. Integrated Seismic and Well-Log Analysis for the Exploration of Stratigraphic Traps in the Carbonera Formation, Llanos Foreland Basin of Colombia. J South Am Earth Sci 104, 1–27. https://doi.org/10.1016/j.jsames.2020.102607

Wagoner, J.C. Van, Mitchum, R.M., Campion, K.M., Rahmanian, V.D., 1990a. Siliciclastic Sequence Stratigraphy in Well Logs, Cores, and Outcrops: Concepts for High-Resolution Correlation of Time and Facies, AAPG Methods in Exploration Series. The American Association of Petroleum Geologists, Tulsa.

Wagoner, J.C. Van, Mitchum, R.M., Campion, K.M., Rahmanian, V.D., 1990b. Integrated Seismic and Well-Log Analysis for the Exploration of Stratigraphic Traps in the Carbonera Formation, Llanos Foreland Basin of Colombia, 7th ed, AAPG Methods in Exploration Series. The American Association of Petroleum Geologists, Oklahoma.

Walker, R.G., James, N.P., 1992. Facies Models Response to Sea Level Change, 2nd ed. Geological Association of Canada, Ontario.

Wang, H., Shao, L., Hao, L., Zhang, P., Glasspool, I.J., Wheeley, J.R., Wignall, P.B., Yi, T., Zhang, M., Hilton, J., 2011. Sedimentology and Sequence Stratigraphy of The Lopingian (Late Permian) Coal Measures in Southwestern China. Int J Coal Geol 85, 168–183. https://doi.org/10.1016/j.coal.2010.11.003

Xu, X., Shao, L., Fu, Y., Wang, D., Cai, H., Qin, J., Hou, H., Zhao, J., 2020. Sequence Palaeogeography, Lacustrine Basin Evolution, and Coal Accumulation in the Lower Cretaceous Fuxin Continental Faulted Basin, China. Geological Journal 55, 1195–1215. https://doi.org/10.1002/gj.3483

Zhang, L., Yan, D., Yang, S., Mangi, H.N., Fu, H., Wang, G., Yang, X., Zhang, B., Li, T., Liang, W., She, X., 2020. Effects of Sequence Stratigraphy on Coal Characteristics and CH4 Adsorption Capacity of the Low-Rank Coal in Santanghu Basin, China. J Nat Gas Sci Eng 81, 103467. https://doi.org/10.1016/J.JNGSE.2020.103467